Mutual Influence of Cyclopentadienyl and Carbonyl Ligands in Cymantrene: QTAIM Study

Alexandra O. Borissova, Mikhail Yu. Antipin, and Konstantin A. Lyssenko*

X-ray Structural Centre A.N., Nesmeyanov Institute of Organoelement Chemistry, 28 Vavilov Street, 119991, Moscow (Russia)

Received: June 22, 2009; Revised Manuscript Received: August 20, 2009

The phenomenon of bond length alternation in the cyclopentadienyl (Cp) ligand of cymantrene (η^5-C_5H_5)$Mn(CO)_3$ was investigated using high-resolution X-ray diffraction analysis (XRD) and quantum chemical calculations. It was shown that the *trans*-effect of strong field CO ligands causes the redistribution of electron density in the Cp ring, and it manifests in atomic charges and energy of its carbon atoms. The angle C(Cp)−Mn−CO is characteristic for this feature and can be used for the prediction of bond lengths and the charge distribution in the aromatic fragment in various piano-stool-type complexes.

Introduction

The phenomenon of the *trans*-effect,[1] i.e., the mutual influence of ligands (L) in a complex regardless of the L nature and the type of M−L bonding, is widely studied. At the same time, the variation of geometry and charge distribution in π-bonded systems as a function of ligand involved in the *trans*-effect is almost unknown. Its influence is considered rather weak because of the multicenter character of the M−Cp bond and the application of integral characteristics like the M···Cp separation for the analysis of such systems (see ref 2 and references therein). Furthermore, the detailed analysis of subtle effects of charge distribution in these complexes is usually complicated by the high libration and/or disorder of the Cp ring.[3] Although there are some examples of the *trans*-effect disturbing symmetry of a π-bonded fragment or even changing the type of bonding with a π-ligand,[4] the numerous investigations of sandwich complexes lead to the common knowledge of bond length equalization in the cyclopentadienyl ring (see refs 5 and 6 and references therein). The available data on breaking the D_{5h} symmetry of the Cp ring in MCp_2 complexes can easily be explained by Jahn−Teller effects.[7] The influence of such weak factors as the *trans*-effect on the aromatic fragments, however, is poorly studied.

The above concept fails to describe the behavior of an aromatic ring in three-legged piano-stool compounds, like cymantrene (Figure 1). This molecule differs from the sandwich complexes Cp_2M and Bz_2M (Bz = C_6H_6) with their D_{5h} (D_{5d}) and D_{6h} (D_{6d}) symmetry because the C_{5v} local symmetry of the "upper" part and C_{3v} of the "lower" part in $CpMn(CO)_3$ have only one generic element, a symmetry plane. Hence, the local symmetry of CpMn or $Mn(CO)_3$ fragments should certainly violate its possible highest symmetry. This allows us to question the charge delocalization in the Cp ligand, which was shown in a first structural investigation of $CpMn(CO)_3$ performed by Berndt and Marsh.[8] Indeed, Fitzpatrick et al.[9] reinvestigated the cymantrene structure and performed the additional vibrational study in solution, showing that $Mn(CO)_3$ does not violate C_{3v} local symmetry, while the Cp fragment is significantly distorted from a regular pentagon according to both spectroscopic and structural data. The investigation of Berndt and Marsh[8] failed to detect this distortion since the effect is very subtle, and at that time the experimental opportunities of an X-ray diffraction analysis were too poor to resolve them. The Fitzpatrick analysis of bond lengths, thermal ellipsoids, and IR spectra of Cp-$Mn(CO)_3$ allowed concluding that the observed variation of bond lengths in the Cp ring is due to the peculiarities of M−Cp bonding rather than an accident or an experimental error.

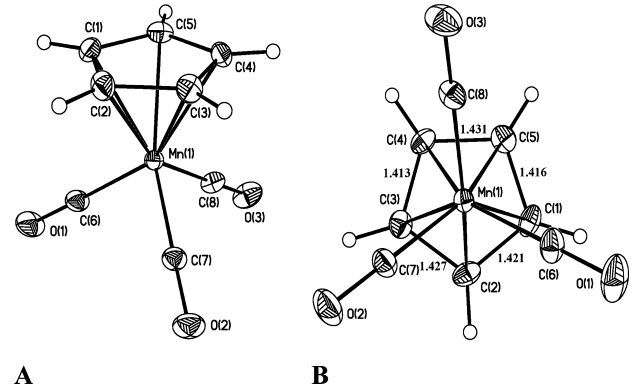

A **B**

Figure 1. General view of the $CpMn(CO)_3$ molecule in two projections with their presentation of atoms by thermal ellipsoids at the 50% probability level and C−C bond lengths in Å.

Our aim was to clarify the reasons of this phenomenon via a detailed analysis of the charge density distribution function $\rho(\mathbf{r})$ in both the isolated cymantrene molecule and its crystal. The charge density distribution was analyzed within Bader's "Atoms in Molecules" (AIM) theory.[10] The latter gives direct information on the presence and type of chemical bonds in a crystal.[11] Moreover, during the last years, a number of investigations[12] demonstrated that application of topological analysis of the $\rho(\mathbf{r})$ derived from experimental data and/or from ab initio calculations in conjunction with Espinosa's correlation scheme[13] allows estimating the interaction energy (E_{cont}) with sufficient accuracy. In particular, the reliability of this approach has recently been demonstrated for the analysis of the bonding pattern in π-complexes in the case of (η^6-$C_6H_6)_2Cr$[14] and Cp_2Ru.[5]

The experimental $\rho(\mathbf{r})$ function obtained from high-resolution X-ray diffraction data provides the additional opportunity to analyze the peculiarities of crystal packing. The latter not is

* Corresponding author. E-mail: kostya@xray.ineos.ac.ru. Fax: (+7495)1355085.

10.1021/jp905841r CCC: $40.75
Published on Web 09/15/2009

TABLE 1: Details of the Data Collection and Refinement of $CpMn(CO)_3$

	$CpMn(CO)_3$
M	204.06
T	100(2) K
space group	*P*21/*n*
a, Å	10.7512(5)
b, Å	6.9258(3)
c, Å	11.6465(5)
b, °	115.7940(7)
V, Å^3	780.80(6)
Z	4
density, g cm^{-3}	1.736
μ (Mo Kα), mm^{-1}	1.646
F(000)	408
diffractometer	SMART APEX2 CCD
absorption correction (Mo Kα)	semiempirical from equivalents
scan technique	ω-scan with 0.5 step
θ_{max}, °	56
number of collected reflns	106449
number of independent rflns (R_{int})	10350 (0.0267)
number of observed rflns with $I > 2\sigma(I)$	8478
conventional refinement	
w*R*2	0.0632
*R*1	0.0231
GOF	1.001
ρ_{max}/ρ_{min}, eÅ^{-3}	0.921/−0.736
multipole refinement	
number of rflns with $I > 3\sigma(I)$	5130
R	0.0140
wR	0.0111
GOF	0.9487
ρ_{max}/ρ_{min}, eÅ^{-3}	0.132/−0.234

only interesting in a structural chemistry aspect but also makes it possible to analyze the molecule's behavior in a polar medium that is closer to the solution than to an isolated molecule in ab initio calculation (see, e.g., ref 15).

At the same time, it is very difficult to investigate the bonding between the metal and π-ligand because of the area of flat $\rho(\mathbf{r})$ and low $\nabla^2\rho(\mathbf{r})$ values between them. This feature causes the uncertainty in searching for bond critical points, and the authors of ref 2 use it to explain the phenomenon of short nonbonding and long bonding interactions. One can, however, relate the problems of CP localization to the mutual influence of the ligands (see, e.g., ref 4).

Experimental Section

X-ray Diffraction Analysis. X-ray diffraction data for the single crystals of cymantrene were collected using a "Bruker SMART APEX2" CCD diffractometer. The obtained images were integrated.[16] The precise unit cell dimensions and errors were determined. The absorption correction was applied semiempirically using the SADABS program.[17] The details of X-ray data collection and the subsequent refinement are listed in Table 1. Initially, spherical atom refinements were undertaken with SHELXTL PLUS 5.0[18] using the full-matrix least-squares method. All non-hydrogen atoms were allowed to have an anisotropic thermal motion. Atomic coordinates, bond lengths, angles, and thermal parameters have been deposited at the Cambridge Crystallographic Data Center (CCDC) with number 729870.

The experimental charge density in the crystal was obtained by the multipole refinement based on the Hansen−Coppens formalism[19] using the XD program package.[20] Before the refinement, the C−H bond distances were fixed to the ideal value of 1.08 Å to cope with the well-known shortening of the C−H bond length in X-ray diffraction experiments.[21] The refinement was carried out with electroneutrality constraints. The multipole expansion was truncated to hexadecapole for the Mn atom, octopole for carbon and oxygen atoms, and dipole for H atoms. The refinement was carried out against F, and the multipole occupancies of all atoms were refined without any local symmetry constraints. The results of the multipole refinement are listed in Table 1. The κ and κ' values as well as the multipole populations are summarized in the Supporting Information. All bonded pairs of atoms satisfy the Hirshfeld rigid-bond criteria.[22] The final residual Fourier maps for cymantrene were flat and featureless (see Supporting Information). Analysis of deformation electron density and topology of the $\rho(\mathbf{r})$ function as well as the calculation of ELF was carried out using the WINXPRO program package.[23]

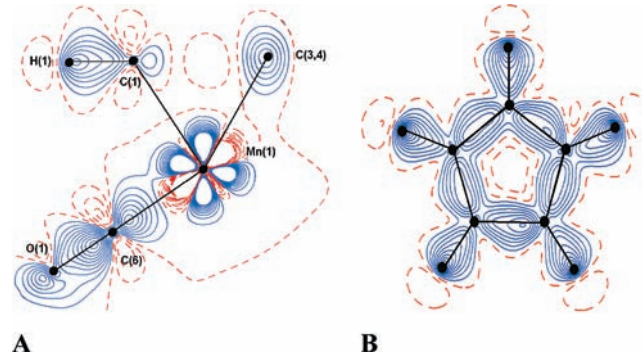

Figure 2. DED maps in the area of (A) vertical section including C(1), C(6), O(1), and Mn(1) atoms and (B) Cp ring. The contours are drawn with 0.1 eÅ^{-3} steps; the positive contours are blue; and the negative contours are red and dashed. The C(3,4) is the middle of the C(3)−C(4) bond in the ring.

Quantum Chemical Calculations. The calculation of the $CpMn(CO)_3$ molecule was performed with the Gaussian 98 program package.[24] The DFT calculation was carried out at the B3pw91 level using a 6-311+G(d,p) basis set. As convergence criteria, the extremely tight threshold limits of $2\cdot10^{-6}$ and $6\cdot10^{-6}$ au were applied for the maximum force and displacement, respectively. To enhance the accuracy in the DFT calculation, the pruned (99 590) grid (keyword Grid = Ultrafine) has been used. The RMP2-FC optimization was performed using a 6-311+G(d,p) basis set. The optimized geometry of $CpMn(CO)_3$ is close to the experimental one in the case of DFT calculation, whereas the MP2 level of theory gives unsatisfactory results in terms of both geometry and charge distribution. The topological analysis of the $\rho(\mathbf{r})$ functions was performed using the AIMAll program package,[25] based on the wave functions obtained from the above calculations.

CSD Search. The data were recovered from the November 2008 update release of the CSD (version 5.30),[35] where both neutral and charged species were taken into account. Only entries with atomic coordinates avaliable and $R < 0.10$ were considered. The results of these searches are discussed below and presented in a histogram form (see Figure 7). The C(2)−Mn(1)−C(8) angles in cymantrene derivatives were searched, and such a subset of structural data was created.

Results and Discussion

The molecular geometry of the $CpMn(CO)_3$ moiety (Figure 1) is similar to that described in ref 9. The local symmetry of the molecule in crystal is C_1. Although the Mn−C (Cp) bond lengths are close to each other (the largest deviation from the

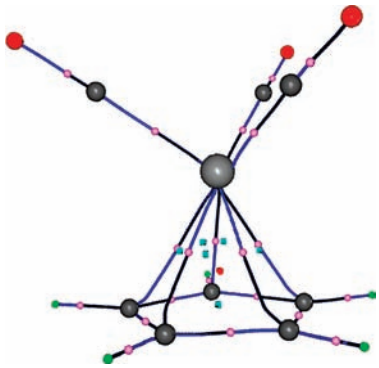

Figure 3. Molecular graph of the $CpMn(CO)_3$ molecule. CPs(3,−1), pink points; (3,+1), blue points; and (3,+3), red point in the $CpMn(CO)_3$ molecule.

average value is 0.0027(4) Å), the C−C bond length differences are significant enough to interpret this as evidence of bond localization in the Cp ring (Table 2). The shortest C−C bonds are C(1)−C(5) and C(3)−C(4) (Figure 1), which differ from the others by 0.0177(6) Å. We draw your attention to the high quality of the performed experiment; the error lies in the fourth digit after point. Therefore, we can consider the above values reliable enough to interpret such subtle effects since the librational corrections of C−C bonds are as small as 0.003 Å. The geometry-based HOMA aromaticity index,[26] which is equal to 0.69 for the Cp ring in $CpMn(CO)_3$, also indicates the nonequivalence of the C−C bonds. For comparison, the high-resolution structural investigation of the Cp_2Ru crystal[5] shows a largest difference in C−C bond lengths of 0.0030(5) Å, which is evidence of complete electron delocalization in the Cp ring. The bond distance variation of 1.415−1.429 vs 1.4135(6)−1.4312(6) Å in the Cp ring of $CpMn(CO)_3$ has independently been shown by DFT calculations (1.415−1.429 vs 1.4135(6)−1.4312(6) Å), which indicate a shortening of the same C(1)−C(5) and C(3)−C(4) bonds. Unfortunately, an MP2 calculation that was performed failed to reproduce the effect of bond length alternation—the optimized geometry of the Cp ring is almost a regular pentagon with C−C bond lengths varying in the range of 1.431−1.435 Å. The equalization of bond lengths in the MP2 calculation is a consequence of the significant shortening of the metal−centroid distances, which are 1.772(1) and 1.777 Å according to XRD and DFT against 1.650 Å in the case of MP2. The M−CO distances at the MP2 level are also significantly shortened, −1.7973(4) (XRD), 1.789 (DFT), and 1.683 Å (MP2). Hence, the DFT calculation reproduces the experimental charge density distribution in the cymantrene molecule, while the MP2 calculation does not. Despite this, in the further discussion we will use both the DFT and MP2 results because the latter shows the hypothetical cymantrene molecule with equal Cp bond lengths that is suitable model for comparison.

As can be seen from the deformation electron density (DED) map in a vertical section including carbon and manganese atoms (Figure 2a), two DED maxima in the vicinity of the metal atom are directed perpendicular to the Cp ring (one to the center of the Cp ring and another one to the center of oxygen atoms triangle), and two others are almost parallel to the Cp ring. The areas of DED depletion are directed along the Mn−C bonds. The principal characteristics of the charge density distribution in the Cp ring (Figure 2b) are close to the expected ones: the charge accumulation is observed for all the chemical bonds, and all carbon atoms seem to be almost equivalent. These main characteristics of the electron density distribution are in good agreement with available data.[2,5,6]

The topology of the $\rho(\mathbf{r})$ function is identical for the crystal and the isolated molecule of cymantrene. The critical point (CP) search revealed the presence of CPs(3,−1) for all observed Mn−C, C−C, C−O, and C−H bonds, a CP(3,+1) for the Cp ring, five CPs(3,+1) for the three-membered MnC_2 ring, and a CP(3,+3) for the MnC_5 polyhedron (Figure 3). It should be noted that the CPs(3,+3) can not be located in ab initio calculations of Cp_2Fe and Bz_2Cr due to extremely small distances between the CP(3,+3) of the cage and the CP(3,+1) of the π-ligand. The reason is the extremelty small M···Cp separation in the latter compounds—about 1.61 and 1.65 Å, respectively. In the cymantrene, however, this distance is about 1.77 Å, and thus, increase of the M−π-ligand separation (of about 0.1 Å) is enough to allow separating the cage critical point of the MC_5 polyhedron and the ring critical point of the five-membered ring; the distance between them is 0.77 Å.

The topological parameters of $\rho(\mathbf{r})$ at CPs(3,−1) of Mn−C and C−C bonds for the experimental and theoretical $\rho(\mathbf{r})$ are given in Table 2 and agree with the recent data.[2,27] As expected, the C−C, C−O, and C−H bonds correspond to shared type of interatomic interactions. The CPs of the polar C−O bonds are shifted toward the carbon atoms.[28]

The Mn−C bonds correspond to an intermediate type. They are almost equivalent according to the bond lengths and $\rho(\mathbf{r})$, $\nabla^2\rho(\mathbf{r})$, and $h_e(\mathbf{r})$ values at the respective CPs, but the ellipticity values are considerably different (see Table 2). The ellipticity of the Mn(1)−C(2) bond is higher, so this bond should be weaker than the others. The Mn−CO and C−O bonds are almost linear—their ellipticity values are very small (second decimal place). The C−C bond ellipticities show modest variation of 0.13 with the largest curvature for the C(2)−C(3) bond and the smallest one for the C(4)−C(5) bond (see Table 2).

According to our data, in both the isolated state and the crystal, the cyclopentadienyl ligand has η^5 coordination, despite the recent electron density analysis by Farrugia et al. which showed that its hapticity is four.[2] According to ref 2, this difference is related to the peculiarities of the $\rho(\mathbf{r})$ distribution in π-complexes discussed above and shows that the variation of the refinement procedure can lead to a different bonding graph even in such a simple molecule due to the small curvature of the $\rho(\mathbf{r})$ function. The comparison of the CP(3,−1) topological parameters between those reported in ref 2 and our data (Table 2) shows that the critical point of the Mn(1)−C(2) bond, which in our case is characterized with the highest value of ellipticity, was not located in the experimental data presented by Farrugia et al. On the other hand, Bader's computational study[29] of $HSiCl_3$ and $CpMn(CO)_2$ adduct revealed the presence of five Mn−C(Cp) CPs(3,−1). The topological parameters of the CP for the Mn(1)−C(2) bond are close to the other four, and even the λ_2 Hessian eigenvalue bond CP, which can serve as a measure of CP instability, does not deviate much from the λ_2 of the other Mn−C bonds. The λ_2 values of the CP(3,−1) for Mn(1)−C(2), Mn(1)−C(3), and Mn(1)−C(4) bonds are close to each other (see Table 2). Thus, the localized critical point of the Mn(1)−C(2) bond should not be neglected since there is nothing unusual or artificial in its parameters.

The values of $\rho(\mathbf{r})$ and $\nabla^2\rho(\mathbf{r})$ functions at CPs(3,−1) are twice as high in the case of Mn−CO than for Mn···Cp bonds (Table 2). To explore the strength of metal to ligand binding we estimated their energy using the Espinosa correlation.[13] Although this correlation was designed for estimating the interaction energy (from available experimental and/or theoretical data) of weak closed-shell interactions, it was shown that it is also valid for a qualitative and semiquantitative description

TABLE 2: Bond Lengths (*d*) and Topological Parameters of $\tilde{n}(\mathbf{r})$ at the CPs(3,-1) of $CpMn(CO)_3$[a]

bond	*d*, Å	$\tilde{n}(\mathbf{r})$, eÅ^{-3}	$\nabla^2\tilde{n}(\mathbf{r})$, eÅ^{-5}	λ_1	λ_2	λ_3	ε[b]	$V(\mathbf{r})$, au	$H_e(\mathbf{r})$, au
Mn(1)−C(1)	2.1448(4)	0.513	5.71	−1.501	−0.383	8.162	2.92	−0.0936	−0.0143
		0.46	6.01	−1.28	−0.17	7.45	6.49	−0.086	−0.0118
	2.149	*0.499*	*5.63*	*−1.644*	*−0.584*	*8.032*	*1.76*	*−0.0900*	*−0.0147*
	2.053	*0.617*	*6.34*	*−2.453*	*−0.523*	*9.304*	*3.69*	*−0.1182*	*−0.0656*
Mn(1)−C(2)	2.1427(4)	0.512	5.49	−1.485	−0.188	7.882	6.89	−0.0908	−0.0142
CP is absent									
	2.151	*0.484*	*6.05*	*−1.717*	*−0.106*	*7.870*	*15.56*	*−0.0889*	*−0.0131*
	2.050	*0.628*	*5.95*	*−2.515*	*−0.779*	*9.256*	*2.23*	*−0.1160*	*−0.0619*
Mn(1)−C(3)	2.1467(4)	0.515	5.60	−1.555	−0.255	8.002	5.09	−0.0906	−0.0140
		0.48	6.16	−1.46	−0.35	7.96	3.13	−0.0904	−0.0133
	2.149	*0.498*	*5.67*	*−1.645*	*−0.533*	*7.900*	*2.07*	*−0.0887*	*−0.0147*
	2.053	*0.618*	*6.26*	*−2.459*	*−0.555*	*9.274*	*3.43*	*−0.1176*	*−0.0649*
Mn(1)−C(4)	2.1450(4)	0.502	5.60	−1.419	−0.250	7.943	4.67	−0.0881	−0.0123
		0.47	6.14	−1.37	−0.02	7.53	89.5	−0.0874	−0.0118
	2.149	*0.493*	*5.78*	*−1.672*	*−0.365*	*7.928*	*5.48*	*−0.0892*	*−0.0141*
	2.052	*0.622*	*6.12*	*−2.482*	*−0.652*	*9.250*	*2.81*	*−0.1168*	*−0.0634*
Mn(1)−C(5)	2.1463(4)	0.515	5.66	−1.543	−0.360	8.147	3.28	−0.0931	−0.0142
		0.47	6.20	−1.45	−0.29	7.94	4.04	−0.0874	−0.0118
	2.150	*0.489*	*5.89*	*−1.673*	*−0.213*	*7.741*	*6.92*	*−0.0881*	*−0.0137*
	2.051	*0.625*	*6.03*	*−2.498*	*−0.719*	*9.247*	*2.48*	*−0.1164*	*−0.0626*
Mn(1)−C(6)	1.7984(5)	0.970	11.07	−4.289	−4.098	20.087	0.06	−0.2648	−0.0750
	1.789	*1.013*	*12.40*	*−4.173*	*−3.943*	*20.491*	*0.06*	*−0.2604*	*−0.0660*
	1.684	*1.377*	*7.30*	*−7.366*	*−7.208*	*21.887*	*0.02*	*−0.3500*	*−0.0758*
Mn(1)−C(7)	1.7914(4)	1.009	11.71	−4.419	−4.361	21.046	0.01	−0.2822	−0.0804
	1.789	*1.014*	*12.40*	*−4.200*	*−3.926*	*20.519*	*0.07*	*−0.2608*	*−0.0661*
	1.683	*1.384*	*7.33*	*−7.333*	*−7.239*	*21.898*	*0.02*	*−0.3505*	*−0.0760*
Mn(1)−C(8)	1.8020(4)	0.979	11.98	−4.467	−4.223	20.666	0.03	−0.2712	−0.0735
	1.789	*1.016*	*12.38*	*−4.248*	*−3.906*	*20.533*	*0.09*	*−0.2609*	*−0.0662*
	1.682	*1.384*	*7.33*	*−7.299*	*−7.289*	*21.918*	*0.01*	*−0.3516*	*−0.0760*
C(1)−C(2)	1.4203(7)	2.038	−15.03	−14.961	−12.293	12.220	0.22	−0.7285	−0.4422
	1.422	*1.961*	*−17.78*	*−14.044*	*−11.476*	*7.729*	*0.22*	*−0.3810*	*−0.2827*
	1.433	*1.924*	*−17.26*	*−13.579*	*−11.200*	*7.527*	*0.21*	*−0.3851*	*−0.1790*
C(2)−C(3)	1.4277(6)	1.964	−13.87	−14.484	−11.408	12.020	0.27	−0.6861	−0.4150
	1.425	*1.957*	*−17.73*	*−13.921*	*−11.436*	*7.767*	*0.22*	*−0.3757*	*−0.2790*
	1.434	*1.924*	*−17.23*	*−13.552*	*−11.201*	*7.522*	*0.21*	*−0.3841*	*−0.1787*
C(3)−C(4)	1.4135(6)	2.051	−15.70	−15.225	−12.581	12.109	0.21	−0.7346	−0.4487
	1.415	*1.985*	*−18.12*	*−14.290*	*−11.525*	*7.652*	*0.24*	*−0.3917*	*−0.2901*
	1.431	*1.931*	*−17.34*	*−13.650*	*−11.224*	*7.539*	*0.22*	*−0.3876*	*−0.1798*
C(4)−C(5)	1.4312(6)	1.976	−13.84	−13.916	−12.183	12.260	0.14	−0.6938	−0.4187
	1.429	*1.937*	*−17.35*	*−13.804*	*−11.401*	*7.803*	*0.21*	*−0.3708*	*−0.2757*
	1.435	*1.917*	*−17.20*	*−13.518*	*−11.200*	*7.523*	*0.21*	*−0.3827*	*−0.1784*
C(1)−C(5)	1.4164(7)	2.035	−14.55	−14.562	−12.292	12.308	0.18	−0.7287	−0.4398
	1.417	*1.978*	*−18.03*	*−14.215*	*−11.508*	*7.676*	*0.24*	*−0.3884*	*−0.2878*
	1.432	*1.931*	*−17.30*	*−13.624*	*−11.211*	*7.536*	*0.22*	*−0.3867*	*−0.1795*

[a] The values for M-Cp bonds include (in order of the lines) XRD data (this work and ref 2), DFT and MP2 results, while for other bonds XRD data (this work), DFT and MP2 results. [b] The value of ellipticity.

of stronger intermediate bonds like short O−H···O interactions and coordination bonds.[5,30] The estimated energy of the Mn···Cp bonding is 143.1 and 139.6 kcal/mol from XRD and DFT data, while the average energy of the Mn−CO bond is 86.0 and 81.6 kcal/mol, respectively. This clearly shows that each of the Mn−C(Cp) bonds (27−29 kcal/mol) is about four times weaker than the Mn−CO bonds. Hence, the latter should have the main influence on the metal atom orbitals. The topological parameters at CPs of the Mn−CO bonds are in good agreement with those in manganese carbonyl[31] and $MnH(CO)_4PPh_3$[32] complexes. According to both the bond length and $\rho(\mathbf{r})$ values, the Mn−CO bonds are stronger in cymantrene than in $Mn_2(CO)_{10}$ and $MnH(CO)_4PPh_3$. The average Mn−CO distances are 1.7973(4), 1.8577, and 1.83 Å, while the mean values of $\rho(\mathbf{r})$ at CP(3,−1) are 1.014, 0.836, and 0.956 eÅ^{-3} for $CpMn(CO)_3$, $Mn_2(CO)_{10}$, and $MnH(CO)_4PPh_3$, respectively.

The atomic charges (*Q*) obtained by integration of $\rho(\mathbf{r})$ within the atomic basins (Ω) surrounded by the zero-flux surface[10] are given in Table 3. The accuracy of the obtained charges can in part be justified by the values of the Lagrangian [$L(\mathbf{r}) = -1/4\nabla^2\rho(\mathbf{r})$] and volumes, obtained by the analogues procedure. In particular, the $L(\mathbf{r})$ value for the Mn(1) atom is quite small, namely, $7.1 \cdot 10^{-5}$.[33] In turn, the sum of the atomic volumes in the crystal (194.61 Å^3) reproduces well the volume of the independent part of the unit cell (195.20(6) Å^3) with an error being only 0.3%.

TABLE 3: Atomic Charges Obtained by Integration of the Experimental and Calculated $\tilde{n}(\mathbf{r})$ Functions

atom	XRD	XRD (from[2])	DFT	MP2
Mn(1)	0.70	0.94	0.89	0.83
O(1)	−1.06	−1.17	−1.14	−1.07
O(2)	−1.06	−1.16	−1.14	−1.07
O(3)	−1.08	−1.23	−1.14	−1.07
C(1)	−0.13	−0.07	−0.10	−0.09
C(2)	−0.22	−0.19	−0.13	−0.10
C(3)	−0.20	−0.22	−0.11	−0.09
C(4)	−0.13	−0.22	−0.12	−0.10
C(5)	−0.15	−0.14	−0.13	−0.10
C(6)	0.81	0.73	0.92	0.78
C(7)	0.84	0.79	0.92	0.77
C(8)	0.83	0.82	0.92	0.77

The charge distribution in the Cp ring shows the nonequivalence of its carbon atoms. The Q values fluctuate within 0.1e, while the value of "charge leakage" (the method error) is 0.01e, so the difference in carbon charges can be regarded as significant. The atom C(2), which is geometrically "distinct" from the others (Figure 1b), has a maximum Q (by the absolute value). Comparing our results with the recently reported data,[2] one can see that the values of the monopole population of the Cp carbon atoms, which can be attributed to their charges, show the same trend as the monopole and Q values in our work—the C(2) atom has the highest monopole population. At the same time, the reported[2] Q values show a different trend with the highest charge at the C(1) atom. We cannot exclude that the absence of the CP(3,−1) in ref 2 for this atom is directly related to the consequent error in determining of the atomic surface and the corresponding atomic charge. Since the net charge of the Cp ring was found to be 0.02e, we can assume that the electrostatic forces give small input into the bonding.

The AIM charge values obtained by integration of the calculated $\rho(\mathbf{r})$ functions (DFT and MP2) are considerably different. DFT calculations do not reproduce the experimental charges but display the same trend of the charge accumulation on the C(2) atom. However, the results of MP2 calculations reveal a charge delocalization in the Cp ring—the charges of all carbon atoms are almost the same, which is consistent with the above C_{5v} geometrical symmetry of the fragment at this level of theory.

Comparison of charges of the oxygen atoms (Table 3) shows that the charge of the O(3) atom in the crystal is slightly higher, apparently, but this difference vanishes in the isolated state. These charge values are affected by the peculiarities of the crystal packing of $CpMn(CO)_3$—since all the oxygen atoms form typical shortened C−H···O contacts with an average C···O distance of 3.311 Å (Figure 4). The CP search in the area of these intermolecular interactions revealed the presence of CPs(3,−1) and the corresponding bond paths in all cases; topological parameters at CPs refer them to closed-shell type. Their interatomic separations and energies estimated via the Espinosa correlation[13] show the reverse trend—the shortest C(1)−H(1)···O(3) interaction has the lowest energy (Table 4). The C(1)−H(1)···O(3) angle is, however, far from 180°, unfavorable for the formation of an interaction and, thus, decreases its energy. The O(1) and O(2) atoms with the lower charges form stronger C−H···O contacts (Table 3).

Several other CPs(3,−1) were located for weaker O···H, O···O, and H···H interactions (see Supporting Information). Their average energy is 0.5 kcal/mol. The carbonyl···carbonyl[34] contacts, which are typical for carbonyl complexes, are absent in the cymantrene crystal. The total energy of the interactions in the crystal of $CpMn(CO)_3$ is 10.3 kcal/mol. As it was proposed recently,[12] this value should give us the sublimation enthalpy of a compound. The experimental sublimation enthalpy of cymantrene is 12.5 kcal/mol, which is in good agreement with the above sum of all interaction energies.

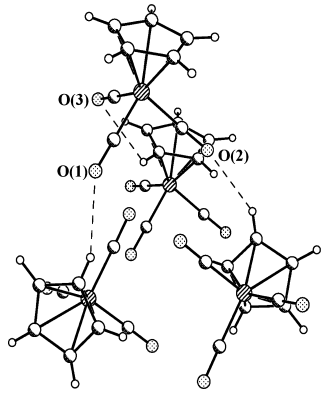

Figure 4. Fragment of crystal packing of $CpMn(CO)_3$ illustrating the C−H···O interactions.

TABLE 4: Parameters of Intermolecular C−H···O Interactions in the Crystal of Cymantrene

	C···O distance, Å	C−H···O angle, °	energy, kcal/mol
C(1)−H(1)···O(1)	3.3354(7)	151.2(9)	1.3
C(4)−H(4)···O(2)	3.3363(6)	150.9(14)	1.4
C(1)−H(1)···O(3)	3.2602(4)	113.6(9)	1.1

TABLE 5: Atomic Energies Obtained by the Integration of the Calculated $H_e(\mathbf{r})$ Functions (dE Is Calculated in Respect to the C(2) Atom)

	DFT		MP2	
atom	E, au	dE, kcal/mol	E, au	dE, kcal/mol
C(1)	−38.014	−1.3	−37.997	3.1
C(2)	−38.012	0	−38.002	0
C(3)	−38.015	−1.9	−37.998	2.5
C(4)	−38.014	−1.2	−38.000	1.3
C(5)	−38.013	−0.6	−38.001	0.6

The comparison of atomic charges in cymantrene with the atomic charges in $Mn_2(CO)_{10}$ obtained using the same procedure[31] showed that the manganese charge is higher in the case of the carbonyl complex, namely, 1.164e vs. 0.70 e in $CpMn(CO)_3$. This agrees with the fact that the Cp ligand can serve as an electron donor for the metal atom orbitals.

The influence of the *trans*-effect on the charge distribution in the Cp ring can be traced not only from the Q values of the carbon atoms but also from the corresponding atomic energies. The deviations of atomic energies relative to the C(2) atom (see Table 5) according to DFT show that all other carbon atoms have significantly lower energies. Moreover, the mutual disposition of the C(Cp) and CO ligands is consequently reflected in the C(Cp) atomic energies (Figure 1, Table 5). The atom C(2), which is in strict *trans*-position to the CO ligand, has the highest energy. The energies of the C(4) and C(5) atoms being slightly shifted from *trans*-position are slightly lower, while the C(1) and C(3) atoms, which are located in nearly eclipsed position, have the lowest-energy values. The MP2 calculations display a totally different trend. When the atomic energies are obtained by integration of the experimental $\rho(\mathbf{r})$ data, they do not vary in the same manner as DFT ones do because this effect is very subtle, and on the level of atomic energies it can be easily influenced by the intermolecular interactions of the carbon atoms involved.

As can be seen from Figure 5, the shortest C(3)−C(4) and C(1)−C(5) bonds are located above the charge density depletion area near the metal atom, while the other bonds, which are considerably longer, are located above the area of its charge accumulation, and the "special" C(2) atom is directly above the negative peak in DED. The $(CO)_3$ fragment "projects" its C_{3v} symmetry onto the d-orbitals of the metal atom, and the DED maxima are located above the CO moieties. The position of the d-orbitals of the metal atom causes the stretching of the C(1)−C(2), C(2)−C(3), and C(4)−C(5) bonds and the compression of the C(1)−C(5) and C(3)−C(4) bonds. The donation from the bonding $1a'^{(2)}$ orbital to Cp* and the back-donation from Cp MOs to antibonding $5a'^{(0)}$ determine the binding between the metal atom and π-ligand. In this respect, the above effect

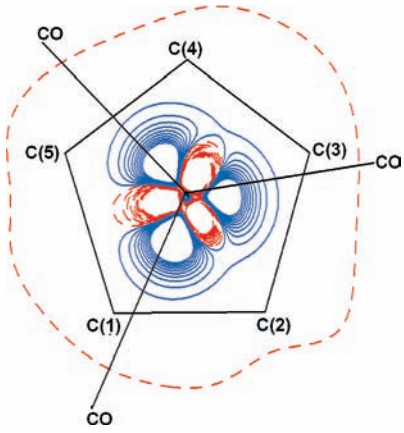

Figure 5. DED map in the plane parallel to the Cp ring and shifted toward Mn(1) by 1.5 Å. The contours are drawn with 0.1 eÅ^{-3} steps. The positive contours are blue, and the negative contours are red and dashed. Black solid lines show the Cp ring and carbonyl groups, which are out of this plane.

can be considered as the experimental evidence of the 5a′→Cp* donation. The DED and ELF (electron localization function) 3D-mapping, which are rather complicated for visualization, reveal the same trend.

The analysis of the C−C bond lengths in the cyclopentadienyl ring of three-legged piano-stool compounds from the CSD[35] showed a similar mutual influence of the ligands. As the available structural data, i.e., the C−C bond lengths in the cyclopentadienyl ring, may be biased due to the libration and even disorder,[36] we focused on the most reliable data—the high-resolution XRD investigations. Recently, Sean McGrady and coauthors reported the experimental charge density distribution analysis of the Mn−SiH bonding in Mn(η^2-SiH) cymantrene derivatives.[37] Since this paper lacks the C(Cp) charges and energies as well as the topological parameters for the MnCp fragment, we can discuss only the precise C−C bond lengths. As can be seen from Figure 7, the C−C cyclopentadienyl bonds located "above" the CO ligand are lengthened in the same manner as in the cymantrene.

To compare our results with the theoretical investigations of three-legged piano-stool compounds, we analyzed the reported benzene(tricarbonyl)chromium molecule.[38] The accurate calculations of both the eclipsed and staggered conformers of $BzCr(CO)_3$ (Figure 6) showed a considerable difference between them. The staggered conformer, which persists in the solid state,[39] displays a considerable alternation of bond lengths in the Cp ring. The bonds, which are in *trans*-position to the CO groups, are shorter (1.414 and 1.396 Å). The eclipsed conformer shows the annealing of bond lengths: the value is in between

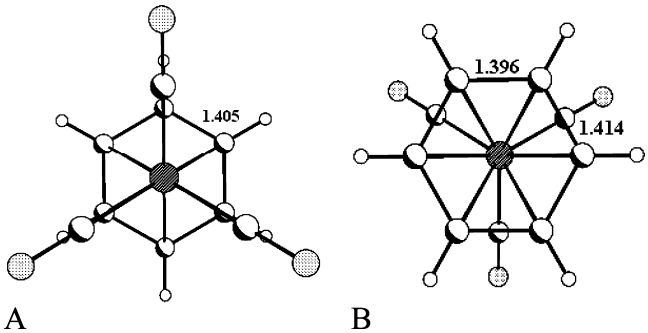

Figure 6. General view of the two conformers of $BzCr(CO)_3$ with C−C bond lengths in Å.

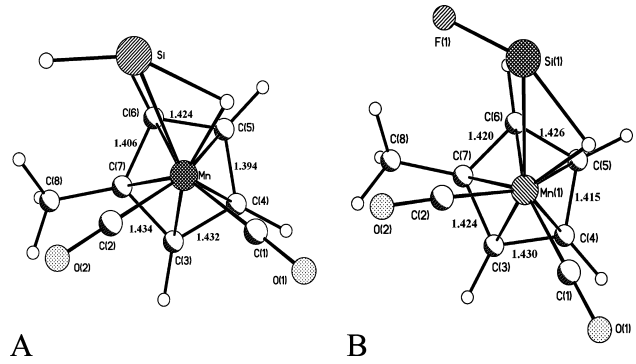

Figure 7. General view of the two Mn(η^2-SiH) cymantrene derivatives with C−C bond lengths in Å.

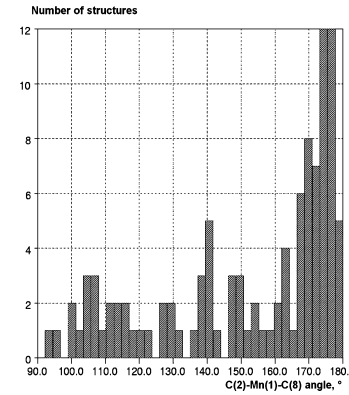

Figure 8. Histogram of the C(2)−Mn(1)−C(8) angle distribution in monosubstituted cymantrene derivatives (C(2) atom is substituted).

the above ones (1.405 Å). In contrast, the values of p_π orbital populations of the carbon atoms of benzene show the opposite trend. They are almost equal in the case of the staggered conformer (0.9967) and alternate in the eclipsed conformer (0.9553 for the eclipsed atom and 1.0390 for uneclipsed one). Taking into account that the latter values can serve as a measure of atomic charge values, we found similar correlations between the CO orientation and bond lengths and charges in the Cp ring of cymantrene. Taking into account the mutual orientation of ligands (Figure 1b) and the above observations about conformers of $BzCr(CO)_3$, one can see that the cymantrene experimental data totally are in perfect agreement with the computational facts. Indeed, the C(3)−C(4) and C(1)−C(5) bonds, which are in *trans*-positions to the CO ligands, are the shortest, while the C(4)−C(5) bond is the longest one. The C(2)−C(3) and C(1)−C(2) bonds are somewhere between. For the atomic charges, we can expect the lowest value for the C(1) and C(3) atoms, the highest one for the C(2), and the intermediate ones for the C(4) and C(5) atoms. Summarizing this with the data of Table 3, we can say that this rule is a general one assuming that the eclipsed orientation is not strictly fulfilled in the case of the cymantrene.

The other important point is that according to the analysis of CSD[35] the substituents of the Cp ring in cymantrene derivatives are mostly antiperiplanar to the CO group. This can be easily seen from the histogram of the C(2)−Mn(1)−C(8) angle (Figure 8). Hence, the direction of substitution is governed by the charge redistribution over the Cp moiety with the accumulation of charge on the C(2) atom. It could be a consequence of steric repulsion, but this is not likely since the distance between the substitute and the carbon atom of the CO group is about 3.5 Å. These results allow interpreting the chemical effect of the observed charge redistribution in the Cp ligand of cymantrene in the directing of substitution reactions. The absence of one of

the Mn−C bond CPs in ref 2 can be a methodological problem of math data processing, but it can have a chemical origin leading to the flatness of electron density between the metal and the Cp ring in π-complexes.

Conclusions

A high-resolution X-ray diffraction investigation of the cymantrene and additional DFT calculation proved the variation of bond lengths in the Cp ring observed earlier. This variation obviously correlates with distribution of the carbon charges and their corresponding atomic energies. By combining these data with the analysis of charge accumulation, which can be attributed to the 3d-orbitals of the metal atom, we showed that the C_{3v} symmetry of the $Mn(CO)_3$ fragment influences the symmetry of the metal d-orbitals and consequently causes the variation of back-donation to the carbon atoms of the Cp ring. Our results show that the angles C−M−CO in three-legged piano-stool compounds can be connected not only to the bond length distribution in aromatic fragment but also to the corresponding carbon charges that can be obtained from high-resolution XRD investigation and/or quantum chemical modeling. Clearly, the correlation of mutual disposition of "legs" with respect to the aromatic fragment in piano-stool complexes can be transferred to other ligands such as phosphines, NO, and C═C moieties. This finding can be used for predicting the stable conformer of substituted piano-stool complexes and can even serve as an additional tool for stabilizing enantiomers in such potentially planar chiral compounds.

Acknowledgment. This study was financially supported by the Russian Foundation for Basic Research (Grants no. 09-03-00603-a, 07-03-00631-a), the Foundation of the President of the Russian Federation (Federal Program for the Support of Young Doctors, Grant MD-172.2008.3). The authors are grateful to Dr. Yu. V. Torubaev (Kurnakov Gen. Inorg. Chem. Inst., Russia) for the preparation of high quality single crystals of $CpMn(CO)_3$.

Supporting Information Available: Tables of monopole, dipole, quadrupole, and hexadecapole populations, table of differences of mean-square displacement amplitudes, full table of atomic coordinates, bond length and angles, integrated values of atomic volumes and charges, and a residual electron density map. This material is available free of charge via the Internet at http://pubs.acs.org.

References and Notes

(1) Coe, B. J.; Glenwright, S. J. *Coord. Chem. Rev.* **2000**, *203*, 5.

(2) Farrugia, L. J.; Evans, C.; Lentz, D.; Roemer, M. *J. Am. Chem. Soc.* **2009**, *131*, 1251.

(3) (a) Braga, D. *Chem. Rev.* **1992**, *92*, 633. (b) Antipin, M. Yu.; Boese, R. *Acta Crystallogr.* **1996**, *B52*, 314.

(4) Bader, R. F. W.; Matta, C. F. *Inorg. Chem.* **2001**, *40*, 5603.

(5) Borissova, A. O.; Antipin, M. Yu.; Perekalin, D. S.; Lyssenko, K. A. *Cryst. Eng. Commun.* **2008**, *10*, 827.

(6) (a) Antipin, M. Yu.; Lyssenko, K. A.; Boese, R. *J. Organomet. Chem.* **1996**, *508*, 259. (b) Lyssenko, K. A.; Antipin, M. Yu.; Ketkov, S.Yu. *Russ. Chem. Bull.* **2001**, *50*, 130.

(7) (a) Lyssenko, K. A.; Golovanov, D. G.; Antipin, M. Yu. *Mendeleev Commun.* **2003**, *13*, 209. (c) Zhen-Feng, Xu.; Yaoming, Xie.; Wen-Lin, Feng; Shaffer, H. F. *J. Phys. Chem. A* **2003**, *107*, 2716.

(8) Berndt, A. F.; Marsh, R. E. *Acta Crystallogr.* **1963**, *16*, 118.

(9) Fitzpatrick, P. J.; le Page, Y.; Sedman, J.; Butler, I. S. *Inorg. Chem.* **1981**, *20*, 2852.

(10) Bader, R. F. W. *Atoms In molecules. A Quantum Theory*; Clarendron Press: Oxford, 1990.

(11) (a) Koritsanszky, T. S.; Coppens, P. *Chem. Rev.* **2001**, *101*, 1583. (b) Gatti, C. *Z. Kristallogr.* **2005**, *220*, 399. (c) Tsirelson, V. G.; Ozerov, R. P. *Electron density and Bonding in Crystals: Principles, Theory and X-Ray Diffraction experiments in Solid State Physics And Chemistry*; IOP Publishing Ltd., 1996. (d) Matta, C. F., Boyd, R. J., Eds. *The Quantum Theory of Atoms in Molecules*; Wiley-VCH: Weinheim, 2007.

(12) (a) Lyssenko, K. A.; Nelyubina, Yu. V.; Kostyanovsky, R. G.; Antipin, M. Yu. *ChemPhysChem* **2006**, *7*, 2453. (b) Lyssenko, K. A.; Korlyukov, A. A.; Golovanov, D. G.; Ketkov, S.Yu.; Antipin, M. Yu. *J. Phys. Chem. A* **2006**, *110*, 6545. (c) Lyssenko, K. A.; Korlyukov, A. A.; Antipin, M. Yu *Mendeleev Commun.* **2005**, 90. (d) Glukhov, I. V.; Lyssenko, K. A.; Korlyukov, A. A.; Antipin, M. Yu. *Faraday Discuss.* **2007**, *135*, 203. (e) Lyssenko, K. A.; Antipin, M. Yu. *Russ. Chem. Bull.* **2006**, *55*, 1. (f) Sobczyk, L.; Grabowski, S. J.; Krygowski, T. M. *Chem. Rev.* **2005**, *105*, 3513.

(13) (a) Espinosa, E.; Molins, E.; Lecomte, C. *Chem. Phys. Lett.* **1998**, *285*, 170. (b) Espinosa, E.; Alkorta, I.; Rozas, I.; Elguero, J.; Molins, E. *Chem. Phys. Lett.* **2001**, *336*, 457.

(14) Lyssenko, K. A.; Korlyukov, A. A.; Golovanov, D. G.; Ketkov, S.Yu.; Antipin, M. Yu. *J. Phys. Chem. A* **2006**, *110*, 6545.

(15) Korlyukov, A. A.; Lyssenko, K. A.; Antipin, M. Yu.; Kirin, V. N.; Chernyshev, E. A.; Knyazev, S. P. *Inorg. Chem.* **2002**, *41*, 5043.

(16) Bruker *SAINT-Plus*; Bruker AXS Inc.: Madison, Wisconsin, USA, 2001.

(17) Sheldrick, G. M. *SADABS*; Bruker AXS Inc.: Madison, WI-53719, 1997.

(18) Sheldrick, G. M. *SHELXTL-97*, version 5.10; Bruker AXS Inc.: Madison, WI-53719, USA.

(19) Hansen, N. K.; Coppens, P. *Acta Cryst. A* **1978**, *34*, 909.

(20) Koritsanszky, T. S.; Howard, S. T.; Richter, T.; Macchi, P.; Volkov, A.; Gatti, C.; Mallinson, P. R.; Farrugia, L. J.; Su, Z.; Hansen, N. K. *XD - A Computer program package for multipole refinement and Topological Analysis of charge densities from diffraction data*; 2003.

(21) Churchill, M. R. *Inorg. Chem.* **1973**, *12*, 1213.

(22) Hirshfeld, F. L. *Acta Cryst. A* **1976**, *32*, 239.

(23) Stash, A.; Tsirelson, V. *J. Appl. Crystallogr.* **2002**, *35*, 371.

(24) Frisch, M. J.; Trucks, G. W.; Schlegel, H. B.; Scuseria, G. E.; Robb, M. A.; Cheeseman, J. R.; Zakrzewski, V. G.; Montgomery, J. A.; Stratmann, R. E., Jr.; Burant, J. C.; Dapprich, S.; Millam, J. M.; Daniels, A. D.; Kudin, K. N.; Strain, M. C.; Farkas, O.; Tomasi, J.; Barone, V.; Cossi, M.; Cammi, R.; Mennucci, B.; Pomelli, C.; Adamo, C.; Clifford, S.; Ochterski, J.; Petersson, G. A.; Ayala, P. Y.; Cui, Q.; Morokuma, K.; Malick, D. K.; Rabuck, A. D.; Raghavachari, K.; Foresman, J. B.; Cioslowski, J.; Ortiz, J. V.; Baboul, A. G.; Stefanov, B. B.; Liu, G.; Liashenko, A.; Piskorz, P.; Komaromi, I.; Gomperts, R.; Martin, R. L.; Fox, D. J.; Keith, T.; Al-Laham, M. A.; Peng, C. Y.; Nanayakkara, A.; Challacombe, M.; Gill, P. M. W.; Johnson, B.; Chen, W.; Wong, M. W.; Andres, J. L.; Gonzalez, C.; Head-Gordon, M.; Replogle, E. S.; Pople, J. A. *Gaussian 98*, revision A.7; Gaussian, Inc.: Pittsburgh (PA), 1998.

(25) Keith, T. A. *AIMAll*, version 08.01.25; 2008, http://aim.tkgristmill.com.

(26) (a) Palusiak, M.; Krygowski, T. M. *Chem.—Eur. J.* **2007**, *13*, 7996. (b) Krygowski, T. M. *J. Chem. Inf. Comput. Sci.* **1993**, *33*, 70.

(27) Cortés-Guzmán, F.; Bader, R. F. W. *Coord. Chem. Rev.* **2005**, *249*, 633.

(28) Macchi, P.; Sironi, A. *Coord. Chem. Rev.* **2003**, *238−239*, 383.

(29) Bader, R. F. W.; Matta, C. F.; Cortés-Guzmán, F. *Organometallics* **2004**, *23*, 6253.

(30) (a) Pidko, E. A.; Xu, J.; Mojet, B. L.; Lefferts, L.; Subbotina, I. R.; Kazansky, V. B.; van Santen, R. A. *J. Phys. Chem. B* **2006**, *110*, 22618. (b) Pidko, E. A.; van Santen, R. A. *ChemPhysChem* **2006**, *7*, 1657. (c) Puntus, L. N.; Lyssenko, K. A.; Antipin, M. Yu.; Bünzli, J.-C. G. *Inorg. Chem.* **2008**, *47*, 11095. (d) Borissova, A. O.; Korlyukov, A. A.; Antipin, M. Yu.; Lyssenko, K. A. *J. Phys. Chem. A* **2008**, *112*, 11519. (e) Nelyubina, Yu. V.; Antipin, M. Yu.; Lyssenko, K. A. *J. Phys. Chem. A* **2009**, *113*, 3615.

(31) Faruggia, L. J.; Mallinson, P. R.; Stewart, B. *Acta Crystallogr.* **2003**, *B59*, 234.

(32) Abramov, Yu.A.; Brammer, L.; Klooster, W. T.; Bullock, R. M. *Inorg. Chem.* **1998**, *37*, 6317.

(33) Grana, A. M.; Mosquera, R. A. *J. Chem. Phys.* **1999**, *110*, 6606.

(34) Sparkes, H. A.; Raithby, P. R.; Clot, E.; Shields, G. P.; Chisholm, J. A.; Allen, F. H. *CrystEngComm* **2006**, *8*, 563.

(35) Cambridge Crystallographic Database, release 2008.

(36) Braga, D. *Chem. Rev.* **1992**, *92*, 633.

(37) (a) Sean McGrady, G.; Sirsch, P.; Chatterton, N. P.; Ostermann, A.; Gatti, C.; Altmannshofer, S.; Herz, V.; Eickerling, G.; Scherer, W. *Inorg. Chem.* **2009**, *48*, 1588. (b) Scherer, W.; Eickerling, G.; Tafipolsky, M.; Sean McGrady, G.; Sirsch, P.; Chatterton, N. P. *Chem. Commun.* **2006**, 2986.

(38) Low, A. A.; Hall, M. B. *Int. J. Quantum Chem.* **2000**, *77*, 152.

(39) (a) Rees, B.; Coppens, P. *Acta Crystallogr.* **1973**, *B29*, 2516. (b) Wang, Yu.; Angermund, K.; Goddard, R.; Kruger, C. *J. Am. Chem. Soc.* **1987**, *109*, 587.

JP905841R